UNIVERSITY OF ILLINOIS

August 10 19 89

THIS IS TO CERTIFY THAT THE THESIS PREPARED UNDER MY SUPERVISION BY

Daniel G. Lis

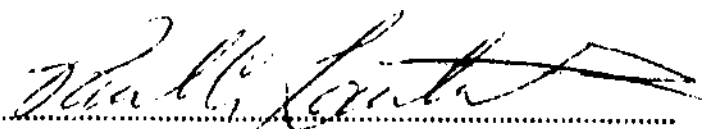ENTITLED Computer Simulation of the Dipole

Artifact in Three-Dimensional NMR Imaging

IS APPROVED BY ME AS FULFILLING THIS PART OF THE REQUIREMENTS FOR THE

DEGREE OF Bachelor of Science in Chemistry

Instructor in Charge

APPROVED:

HEAD OF DEPARTMENT OF Chemistry

O-1364

Computer Simulation of
the Dipole Artifact in Three-Dimensional
NMR Imaging

by

Daniel G. Lis

Thesis

for the
Degree fo Bachelor of Science
i n
Chemistry

College of Liberal Arts and Sciences
University of Illinois
Urbana, Illinois

1989

Contents

Introduction

Since NMR imaging was introduced(1), macroscopic three-dimensional imaging has become a powerful diagnostic tool in the field of medicine. The nondestructive, non-invasive method of obtaining three-dimensional proton density distributions with additional contrast added by T_1, T_2 or diffusion weighting(1,2,3,4,5) promises to be invaluable in clinical diagnosis, including the detection of diseased tissues(1,5). In microscopic NMR imaging resolution is approaching the cellular level due to the availability of specially designed probes allowing greater signal to noise ratios(6).

When the sample contains material of differing magnetic susceptibility, the distortion of the magnetic field in the surrounding material causes a dipole artifact in the final image. In macroscopic imaging such effects might be negligible but at the microscopic level, the resulting image artifact must be eliminated or accounted for to allow an accurate interpretation of the image. The aim of this investigation is to use a computer simulation to produce a set of projections which when reconstructed would allow the determination of the size and susceptibility difference of the artifact's cause.

1

Background

NMR spectroscopy is inherently three-dimensional, all the magnetically active nuclei contained within the volume covered by the excitation and detection coils give rise to a signal. There are several possible methods to spatially encode the resonance signals. Although point and line methods are available, the selective excitation of planes and whole-volume methods are more practical(2). These methods depend on the use of magnetic field gradients (usually linear) to create controlled field inhomogeneities greater than the natural line widths of the resonating signals in the static field. In selective irradiation method, a slice selection gradient is first applied and a narrow band of excitation frequencies is used to induce transverse magnetization in only an isolated slab of the sample. A readout gradient perpendicular to the selection gradient is then applied while the FID is collected. Subsequent Fourier transformation of the FID from the time domain to the frequency domain results in a spectrum that is broadened (due to the gradient) to a shape corresponding to a one-dimensional projection of the sample. This one-dimensional projection consists of line integrals of signal intensity from the successive parallel lines of constant magnetic field. By rotating the gradient in the plane, a set of projections (illustrated in Figure 1) is generated which can be reconstructed to give a two-dimensional image of the object as viewed from along the direction of the rotation axis(8). Successive slices are selected and the whole set of slices are combined to produce the three-dimensional image. Although this method is quicker to produce an image of a given slice, there usually is anisotropic volume resolution due to the difference in the resolution of the slice thickness and the resolution within the plane of the slice(9).

Whole volume imaging methods employ an excitation frequency bandwidth large enough to excite the whole sample. A linear gradient imposed on the static field effectively divides the sample

2

into parallel planes of constant magnetization(10)(Fig. 2). The one-dimensional projections then correspond to the plane integrals of signal intersity from the successive planes of nuclei resonating at the same frequency. By rotating the gradient through θ and ϕ in spherical coordinates, a set of projections is produced from which a complete isotropically resolved three-dimensional image can be reproduced(9).

The dependance on a homogeneous static field modified by a known gradient is key. When a susceptibility difference occurs in the sample, such as an air bubble, the resulting magnetic field disturbance results in a non-planer slice selection in the selective irradiation technique and ultimately geometric distortion and nonuniform pixel intensity in both cases. In the three-dimensional projection reconstruction imaging algorithm, the resulting geometric distortion appears as the well known dipole pattern(11).

Artifact Calculation

Consider a sphere of radius R containing some homogeneous material with relative permeability μ_i surrounded by a second material of relative permeability μ_e. If a coordinate system is chosen as shown in Figure 3 with the static magnetic field in the z direction, the magnetic field inside and outside the sphere can be determined by solving the Laplace equations for the magnetic scalar potential(12). It is shown(13) that the magnetic field inside the sphere is homogeneous and given by

$$B_i = B_0 \left[1 - 2\frac{\mu_e - \mu_i}{2\mu_e + \mu_i}\right] \tag{1}$$

By replacing the permeabilities by susceptibilities according to $\mu = 1 + \chi$ and noting $\chi << 1$ for the common materials involved in NMR experiments, the last term of equation (1) can be expressed as

$$\frac{\mu_e - \mu_i}{2\mu_e + \mu_i} \approx \frac{\Delta\chi}{3} \quad ; \quad \Delta\chi = \chi_e - \chi_i \tag{2}$$

simplifying (1) to

$$B_i = B_0\left[1 - \frac{2\Delta\chi}{3}\right] \tag{3}$$

The independence of spatial coordinates of equation (3) indicate uniform displacement of intensity within the sphere resulting in no geometric distortions in the final image.

4

The external, or dipole field is spatially dependant and sinceonly the component along the static field contributes to frequency shifts in NMR experiments, only the z component is considered and given by

$$B_d = B_o \left[-\frac{\Delta \chi}{3} R^3 \frac{2z^2 - x^2 - y^2}{r^5} \right], \quad \text{where } r^2 = x^2 + y^2 + z^2. \quad (4)$$

In spherical coordinates, equation (4) becomes

$$B_d = B_o \left[1 - \frac{\Delta \chi}{3} R^3 \frac{3\cos^2\theta - 1}{r^3} \right]. \quad (5)$$

Since equation (5) is independent of ϕ, B_d is shown to be cylindrically symmetric about the z axis. Examining equation (5) to determine where the dipole contribution goes to zero yields

$$B_d = 0 \text{ when } 3\cos^2\theta - 1 = 0, \text{ or}$$

$$\text{when } \theta = \cos^{-1}\sqrt{\frac{1}{3}} = 54.7°$$

A contour plot of any plane containing the z axis (Fig. 4) shows the major features of the dipole pattern. The lines at a 54.7° angle with the z axis (the "magic angle") divide regions of positive B_d along the z axis from the negative regions along the perpendicular radial axis.

In the presence of a gradient G(r) (r being the vector along the gradient direction originating at the null point of the gradient), the total field inside the bubble is given by

$$B_{i,T} = B_i + Gr = B_0 \left[1 - \frac{2}{3} \Delta\chi \right] + Gr, \tag{6}$$

and the resonance frequency is given by

$$\omega_i = \gamma (B_0 + Gr) - \frac{2}{3} \gamma B_0 \Delta\chi, \tag{7}$$

Since the first term on the right-hand side of equation (7) is the resonance frequency in the absence of the susceptibility effect (defined as $\omega_{0,i}$), the frequency shift along the gradient direction is given by

$$\omega_i - \omega_{0,i} = -\frac{2}{3} \gamma B_0 \Delta\chi . \tag{8}$$

Since the internal field is homogeneous, the resulting image shift occurs without geometric distortion. Moreover, since there is no detectable spin intensity inside the air bubble, the image shift is not visible in this particular case.

A similar treatment of the external field yields

$$B_{e,T} = B_0 \left[1 - \frac{1}{3} \gamma \Delta\chi R^3 \frac{3\cos^2\theta - 1}{r^3} \right] + Gr \tag{9}$$

and

$$\omega_\theta = \gamma (B_0 + Gr) - \frac{1}{3} \gamma B_0 \Delta \chi R^3 \frac{3\cos^2\theta - 1}{r^3} \qquad (10)$$

$$= \omega_{0,\theta} - \frac{1}{3} \gamma B_0 \Delta \chi R^3 \frac{3\cos^2\theta - 1}{r^3}$$

or

$$\omega_\theta - \omega_{0,\theta} = -\frac{1}{3} \gamma B_0 \Delta \chi R^3 \frac{3\cos^2\theta - 1}{r^3} . \qquad (11)$$

The spatial dependance of equation (11) indicates the geometric distortions recognized as susceptibility artifacts observed in reconstructed images. Since the dipole field is zero along the magic angle, the resulting image is not shifted and the true diameter of the sphere can be determined at that angle.

Computer Simulation

In actual three-dimensional projection reconstruction imaging experiments there are several factors which determine the image integrity which were ignored in the computer simulation. These factors include the calibration of field gradients, optimization of the signal to noise ratio, the uniformity of the excitation radiofrequency pulse, the uniformity of the detection pattern of the receiver coils, field distortions due to sample geometry and probe materials, the effects of pulse sequences, the line width broadening due to inherent static field inhomogeneities and natural line width, and spin diffusion(1,6,10). All of these factors were assumed to be ideal resulting in a situation with no limit to resolution except for computer time. Present minimum voxel size attainable experimentally using the projection reconstruction method simulated is $(6.37\mu m)^3$ using a 7.4 gauss/cm gradient in a 4.7 Tesla static field. The spatial resolution and gradient strength used correspond to a frequency sensitivity of ca. 0.1ppm.

The case considered for the simulation was a spherical air bubble of radius R surrounded by a spherical volume of water. Using the volume susceptibilities of $X_{air}=0.0$ and $X_{H_2O}= -10^{-5}$ and solving equation (4) to determine the limit at which the susceptibility difference would shift intensity into the next volume element (ie. $\frac{B_e - B_0}{B_0} = 0.1ppm$) yields

$$\frac{B_e - B_0}{B_0} = -\frac{2}{3} \Delta X \, R^3 \, z^{-3} = 0.1ppm, \qquad \text{for } x=y=0$$

or

$$z = \left[-\frac{2}{3}R^3 \frac{\Delta X}{0.1ppm} \right]^{1/3} = 3.92 \, R,$$

8

and

$$\frac{B_\theta - B_0}{B_0} = -\frac{1}{3} \Delta\chi \, R^3 \, x^{-3} = 0.1\text{ppm}, \qquad \text{for } y=z=0$$

or

$$x = \left[-\frac{1}{3} R^3 \frac{\Delta\chi}{0.1\text{ppm}} \right]^{1/3} = 3.11 \, R \, .$$

This indicated the dipole contribution is negligible after 4R along the z axis and 3R along the x or any perpendicular axis as illustrated in Figures 5a and 5b so the outer sphere of water was chosen to have a radius of 4R. R was chosen to be 100μm which is a reasonable size for a small air bubble trapped in a sample used in NMR microscopy.

For a given projection, the total field at a given point was calculated and a frequency histogram incremented for the intensity contribution at that point. The region inside the air bubble would not contribute any signal so the only contributing magnetic field effect is from the external dipole field. The frequency at each point can be represented by

$$\omega = \gamma B_T = \gamma (B_0 + B_d + Gr_g), \tag{12}$$

The shift, $\omega_S = \dfrac{\omega - \omega_0}{\omega_0}$, where ω_0 is the frequency in field B_0, is given by

$$\omega_S = \frac{B_d}{B_0} + \frac{Gr_g}{B_0}, \tag{13}$$

where r_g is the radius along the gradient at which the plane of

constant gradient field intersects with the spatial point and can be found by solving the point normal form of the plane equation yielding

$$r_g = \frac{x \sin\theta_g\cos\phi_g + y \sin\theta_g\sin\phi_g + z \cos\theta_g}{\sin^2\theta_g\cos^2\phi_g + \sin^2\theta_g\sin^2\phi_g + \cos^2\theta_g} \qquad (14)$$

where θ_g is the angle between the gradient vector and the z axis and ϕ_g is the angle between the x axis and the projection of the gradient vector in the xy plane.

The space was sampled using a Cartesian coordinate grid with a spacing of 6.4μm between points. The frequency histogram consisted of 128 bins of width $G(6.4\mu m)/B_o = 0.100766$ppm and was incremented using the "locate" subroutine(14). To simulate a continuous object and overcome difficulties in sampling spherical geometries with Cartesian coordinates, a two stage three point averaging filter with boundary conditions was applied.

The number of unique projections was greatly reduced by the symmetry of the dipole pattern and the gratuitous choice of total sample geometry. With the null point of the gradient at the origin, two gradient orientations pointing in exactly opposite directions give reversed projections containing no new information. Since the sample volume is cylindrically symmetric, reorienting the gradient from 0° to 90° in θ alone produces the only unique projections. The angle step sizes were chosen to correspond to the experimental methods currently being employed with $\Delta\theta = 3°$ and $\Delta\phi = 6°$ resulting in the need to calculate 31 unique projections and reproducing them appropriately to generate a set of 3542 total projections.

The simulation was written in "C" and run on the National Center for Supercomputing Application's Aliant computer. The projections were reconstructed on a 128^3 array using one stage

filtered back projection on a 800μm field of view resulting in a 244μm^3 voxel size. The final image was processed with a three-dimensional Gaussian filter and displayed on a Sun workstation using the Viewit software package.

Phantom Image

An actual image of an air bubble in a tube of water was obtained by filling an elliptical plastic tube(long axis 1.4mm, short axis 0.9mm) with water and allowing an air bubble to remain in the sample. A Hahn spin echo was used for each gradient orientation. The echo time was 2ms to minimize the diffusion effect and the pulse width for both 90° and 180° was 6μs to secure a homogeneous excitation. Gradient reorientation for a single stage reconstruction was used with $\Delta\theta=3°$ and $\Delta\phi=6°$ resulting in 3542 total projections. The gradient strength was 6.3 Gauss/cm in a 4.7 Tesla static field. The images were reconstructed as 64^3 arrays on a $(3mm)^3$ field of view resulting in a voxel size of$(47\mu m)^3$.

Results and Discussion

A resulting histogram in the absence of the dipole effects with the gradient along the z axis is shown in Figure 6a. The flat region at the center of the projection corresponds to the missing signal intensity due to the air bubble. The resulting histogram when the dipole effect is considered for the same gradient orientation is shown super imposed on the projection without the dipole in Figure 6b. The intensity shifts can clearly be seen which result in the missing intensity in the reconstructed image. This effect can be qualitatively described as the back projected intensities not converging in the reconstruction space. Normally the intensity for a point in the sample space can be represented as intensity along the frequency axis for each projection. During projection reconstruction the intensity is back projected onto an imaging space as shown in Figure 7a. When the intensity is shifted on the frequency axis due to the dipole field, the back projections from the point in the sample space do not converge in the imaging space as shown in Figure 7b and the resulting image has missing intensity at those points. The resultant image of the simulation is shown in Figure 8.

In order to interpret the cause of the susceptibility artifact a correlation between the amount of frequency shift and the reconstructed image spatial distance must be made. Ideally this should be calculated from the inverse transformation of the k-space expression for the imaging time domain signal, but due to the complexity the added perturbation, it would be difficult. An easier way is to begin by examining equation (11). Substituting the frequency difference with the spatial difference by dividing equation (11) by γG yields

$$r' - r = -\frac{1}{3G} R^3 \, \Delta \chi \, B_0 \frac{3 \cos^2\theta - 1}{r^3} \tag{15}$$

By measuring the radius of the region of missing intensity, r', at a

13

given value of θ and measuring the radius of the air bubble at $\theta \approx 54.7°$, the susceptibility difference can be found if the value of r is known.

Using the simulated data r' was measured to be 0.165mm at $\theta = 90°$ using a feature of the display package which allows an intensity profile to be displayed (Figure 9). The measured value of r' was determined by the width of the large intensity well(the smaller well centered in the larger one corresponds to the zero intensity of the air region). Since $\Delta\chi$, G, B_0, and R are known, equation (15) can be solved for r resulting in r=1.92 R. Defining $C \equiv \dfrac{r}{R}$ and measuring r' at 90°, either R or $\Delta\chi$ can be easily found by

$$R = \frac{r' - \frac{1}{3G}\Delta\chi \; B_0 \; C^{-3}}{C} \tag{16}$$

and

$$\Delta\chi = \frac{(r' - r) \; 3G \; C^3}{B_0} \tag{17}$$

where C = 1.92.

Applying this method to the experimental image(Figure 10), R and r' were first measured from the image and found to be 175μm and 315μm respectively. Calculating R using equation (16) resulting in R = 178μm. Then using the experimental R in equation (17) resulted in $\Delta\chi$ = -7.02x10^{-6} cm^{-3} or -10.06x10^{-6} cgs compared to the real values of -9.05x10^{-6} cm^{-3} and -12.97x10^{-6} cgs.

The discrepancies between the simulated image and the experimental image, namely the compression of the torrodial lobe and the absence of marked intensity build up around the edge of the pattern, can be partially explained by the lower resolution of the experimental image. The lower resolution would in effect smear the

edges of the pattern as the signal is averaged over the larger voxel. The distortions near the boundary of the tube(top center and upper .ight in Fig. 10) may be due to smaller air bubbles.

Conclusion

The inverse transform of the **k**-space expression is difficult to apply when determining the image intensity displacement due to a susceptibility difference. A method using the displacement for a particul. gradient orientation can be used once a correlation between the radius(in the same direction of the gradient orientation) of the region of missing intensity in the final image and the original location of the intensity contribution is made. If the radius of the cause of the dipole pattern could be directly measured in the image, the susceptibility difference can easily be calculated, but if the susceptibility difference is already known, an accurate calculation of the diameter of the cause can be made. With the use of magnetite particles as cellular labels(15), this method would allow the accurate determination of the size of the magnetite particle from the dipole pattern even though the particle is smaller than the resolution of the image.

Acknowledgements

17

References

1. Paul C. Lauterbur, "Image formation by Induced Local Interactions: Examples Employing Nuclear Magnetic Resonance", *Nature* **242**:190 (1973).

2. Ching-Ming Lai, Walton V. House, Jr. and Paul C. Lauterbur, "Nuclear Magnetic Resonance Resonance Zeugmatography for Medical Imaging", Presented at Session 30, "Technology for Non-Invasive Monitoring of Physiological Phenomena", ELECTRO/78, Boston Mass., (1978).

3. M. H. Mendonca Dias and Paul C. Lauterbur, "Ferromagnetic Particles as Contrast Agents for Magnetic Resonance Imaging of the Liver and Spleen", *Magnetic Resonance in Medicine*, **3** :328 (1986).

4. M. H. M. Dias and Paul C Lauterbur, "Contrast Agents for Nuclear Magnetic Resonance Imaging", *Biological Trace Element Research* **13**: 229 (1987).

5. Stephan Mann, A. Jerome Skarnulis, Robert J. P. Williams, "Location of Biological Compartments by High Resolution NMR Spectroscopy and Electron Microscopy Using Magnetite-containing Vesicles", *J. C. S. Chem. Comm.* 1067 (1982).

6. Ian L. Pykett, "NMR Imaging in Medicine" *Scientific American* **246**: 78 (1982)

7. Paul C. Lauterbur, Xiaohong Zhou, Clinton C. Potter, Brian Voth, J. C. Alexander, Jr. and Richard L. Magin, "Three-dimensional NMR Microscopy", Abstracts of International Society of Magnetic Resonance, Tenth Meeting, Morzine France, 1989.

8. Paul C. Lauterbur, C. S. Dulcey, Jr., C.-M. Lai, M.A. Feiler, W.V. House, Jr., D.M. Kramer, C.-N. Chen and R. Dias, "Magnetic Resonance Zeugmatography", Magnetic Resonance and Related Phenomena, Proceedings of the 18th Ampere Congress, Nottingham, 9-14 Sept. 11974, edited by P.S. Allen, E. R. Andrew and C.A. Bates, North-Holland, Amsterdam, 1975.

9. C.-M. Lai and Paul C. Lauterbur, "True Three-Dimensional Image Reconstruction by NMR Zeugmatography", *Phys. Med. Biol.*, Vol, 26 No. 5, 851-856.

18

10. Paul C. Lauterbur, "Reconstruction in Zeugmatography: The Spatial Resolution of Magnetic Resonance Signals", Proceedings of the International Workshop on 3D Image Reconstruction Techniques, Brookhaven National Lab., (1974).

11. Paul C. Lauterbur, M.L. Bernardo, Abstracts, 4th Annual Meeting of the Society of Magnetic Resonance in Medicine, London p.742, 1985.

12. B.I. Bleaney and B. Bleany, Electricity and Mangnetism 3rd Ed., Oxford University Press, 1976, p308.

13. K.M. Lüdeke, P. Röschmann and R. Tischler, "Susceptibility Artifacts in MNR Imaging", *Mag. Reson. Imag.* **3**: 323 (1985).

14. Wm. H. Press, Brian P. Flannery, Saul A. Teukolok, Wm. T. Veltring, Numerical Recipes in C, Cambridge University Press, NY, 1988, p. 98.

15. Paul C. Lauterbur, M.L. Bernardo, M.H.M. Dias and L.K. Hedges, Microscopic NMR Imaging of the Magnetic Fields Around Magnetite Particles, Work in Progress Abstract, 5th Annual Meeting of the Society of Magnetic Resonance Imaging in Medicine, 1986.
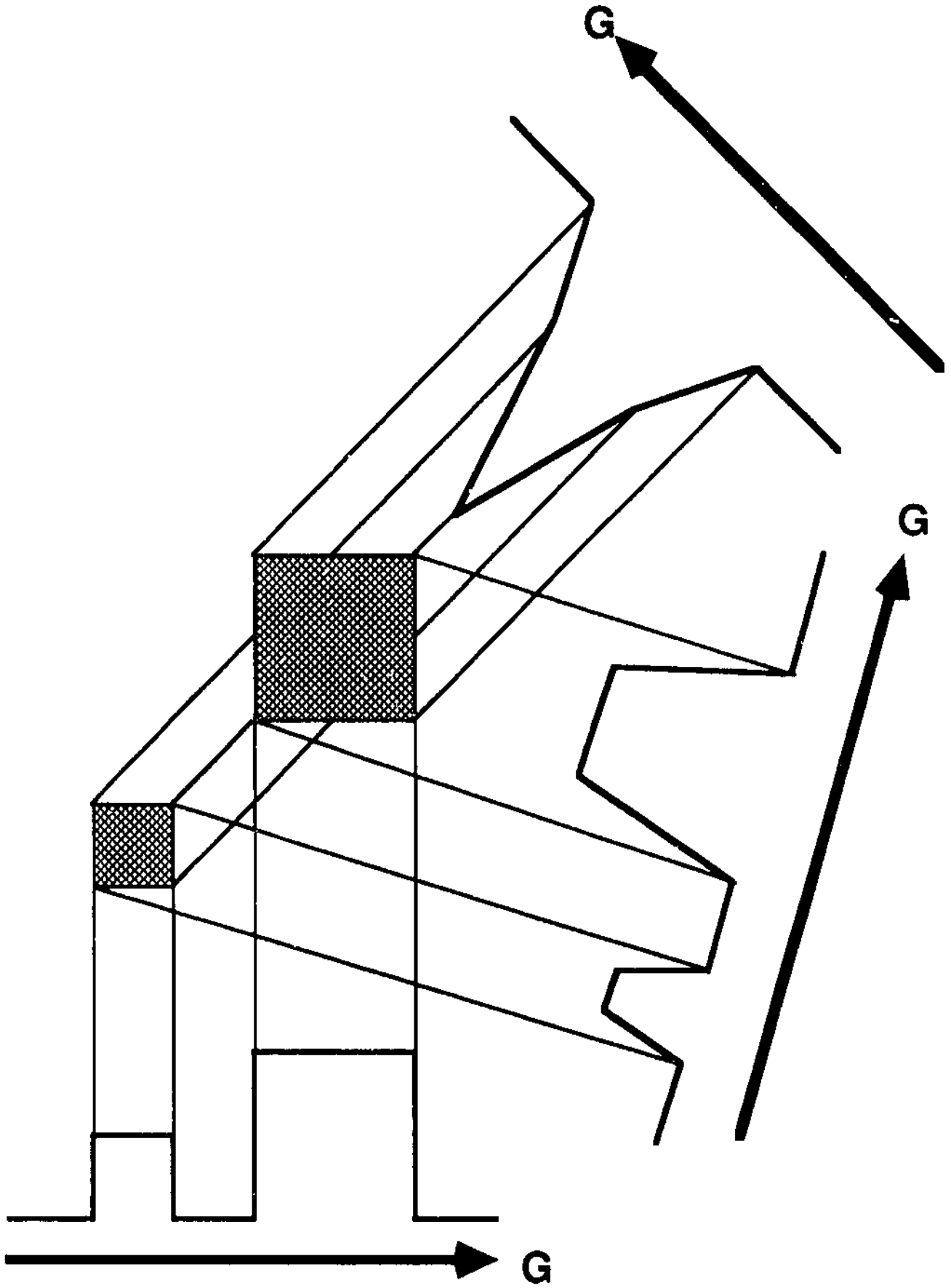
Figure 1: Projections generated for three gradient orientations
in a two-dimensional case
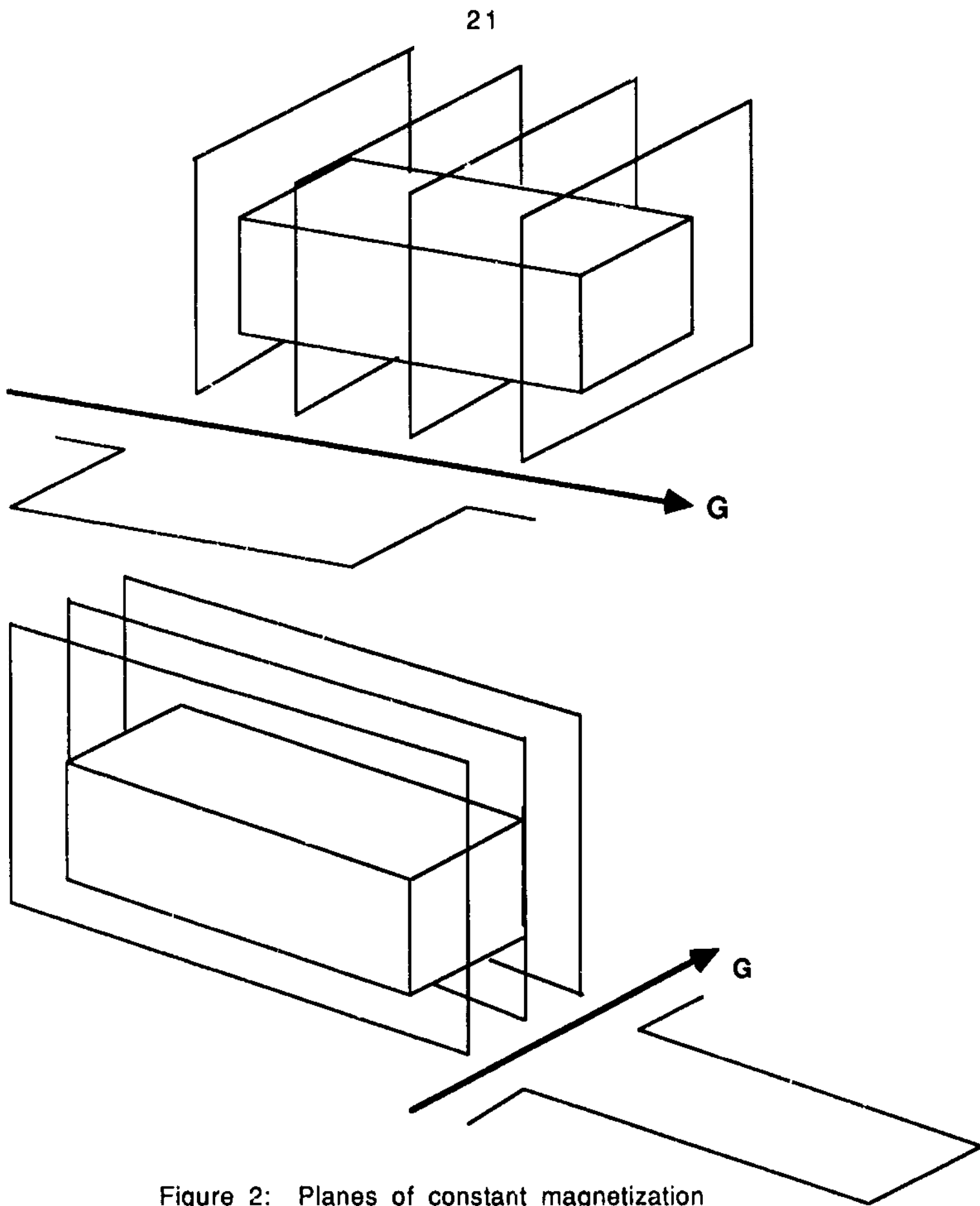
Figure 2: Planes of constant magnetization for two gradient orientations with their appropriate projections.
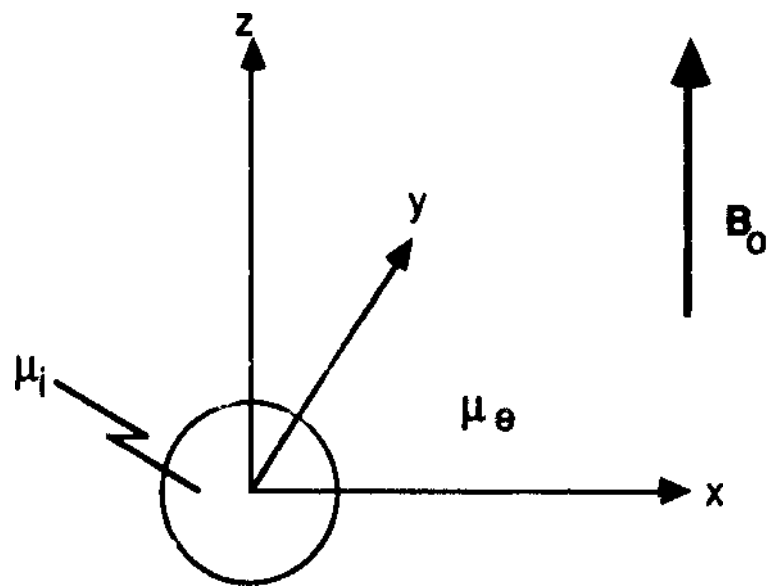
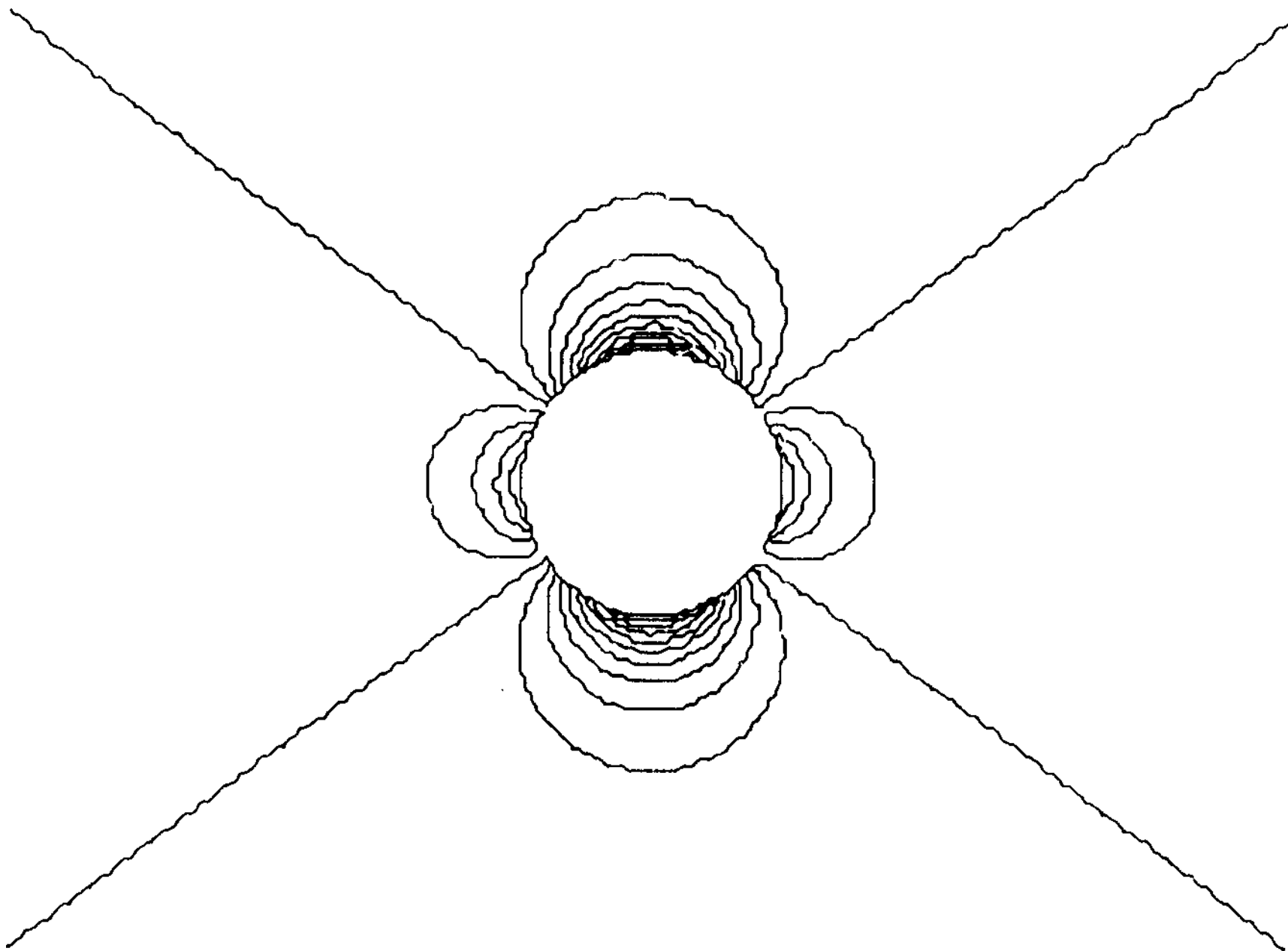Figure 3: Coordinate system for artifact calculation

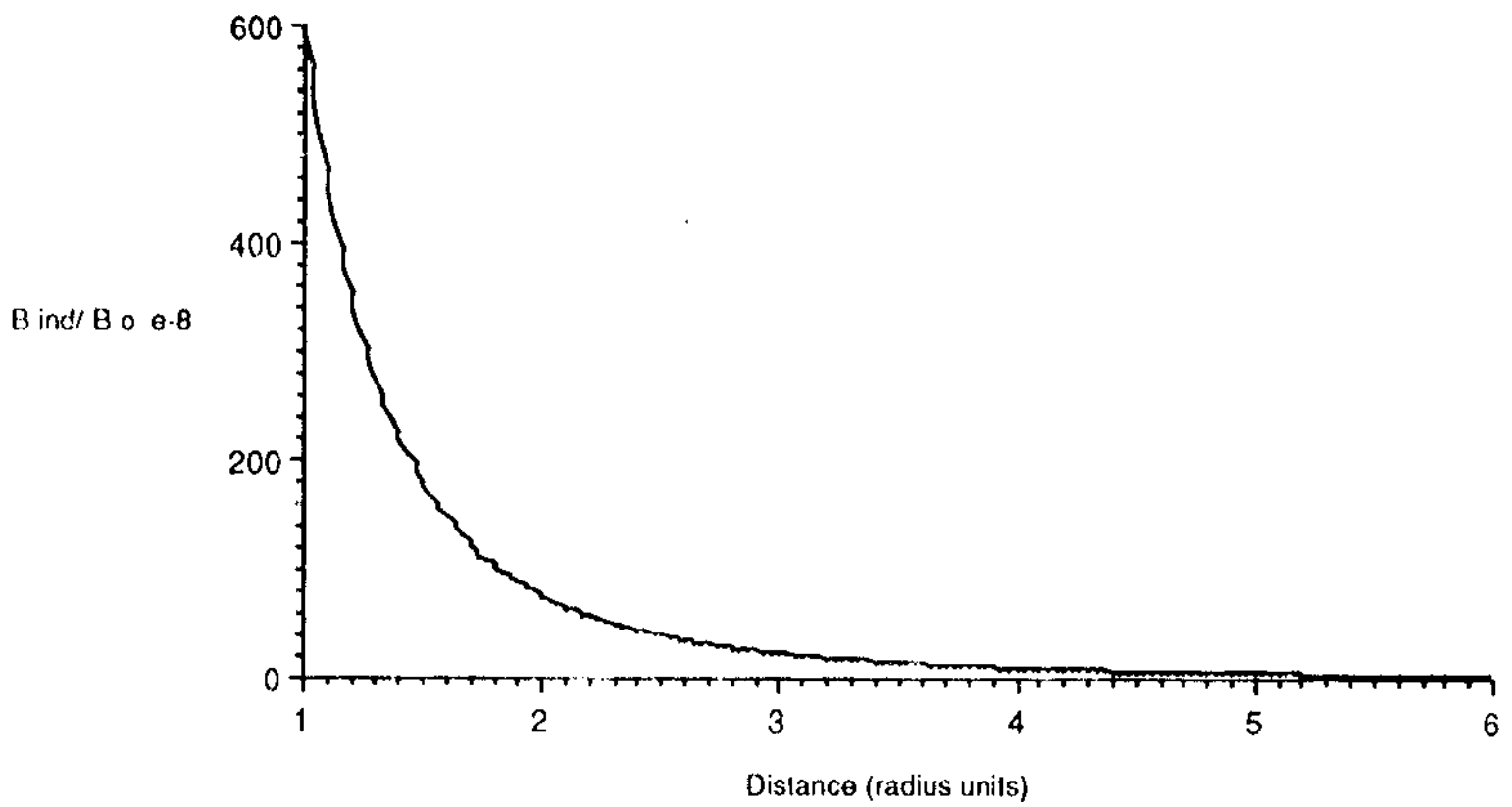Figure 4: Contour plot of logitudinal dipole field with contour spacing of 0.56 ppm of the imposed field.

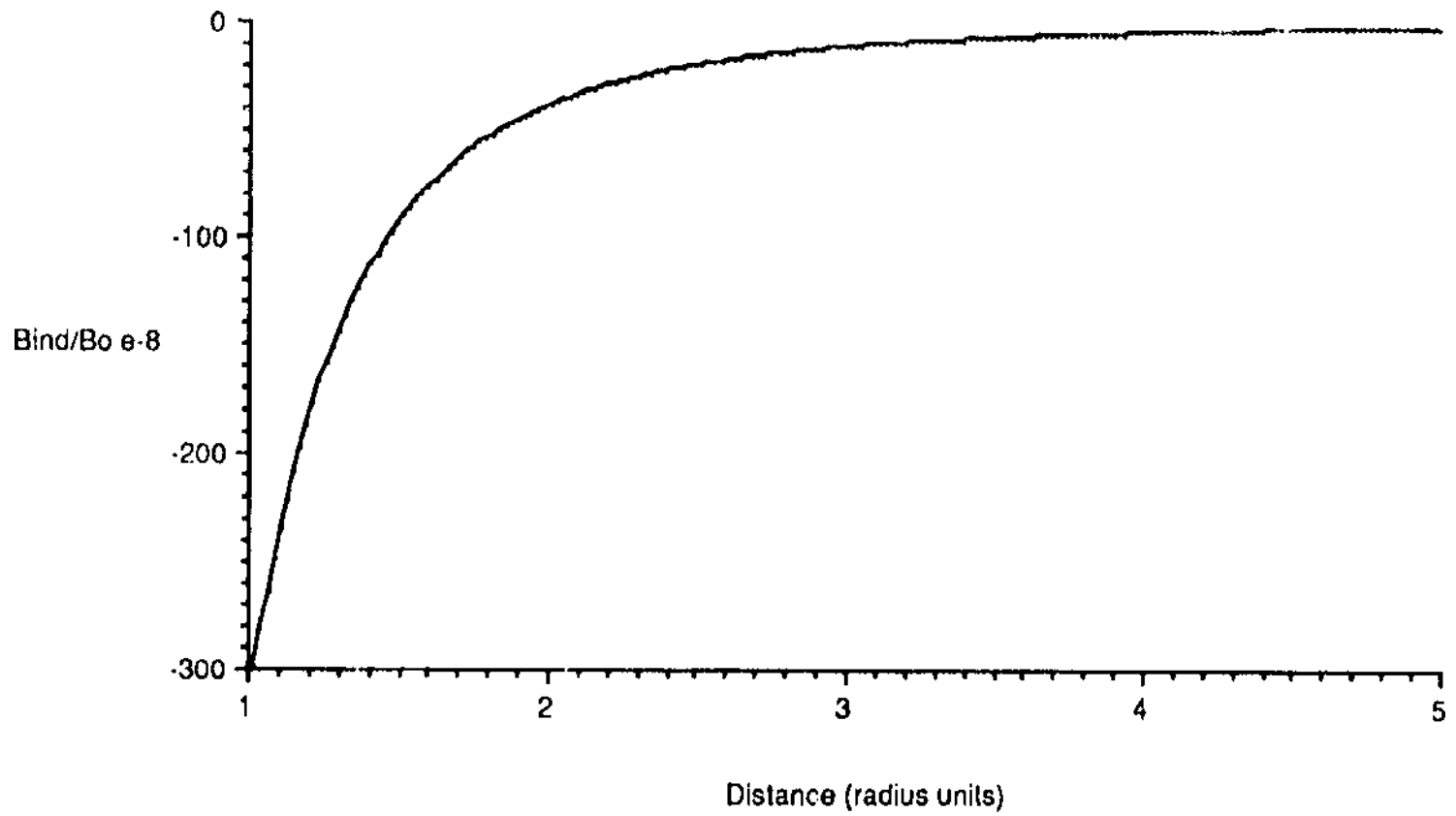Figure 5a: Relative dipole field value vs. distance along z axis

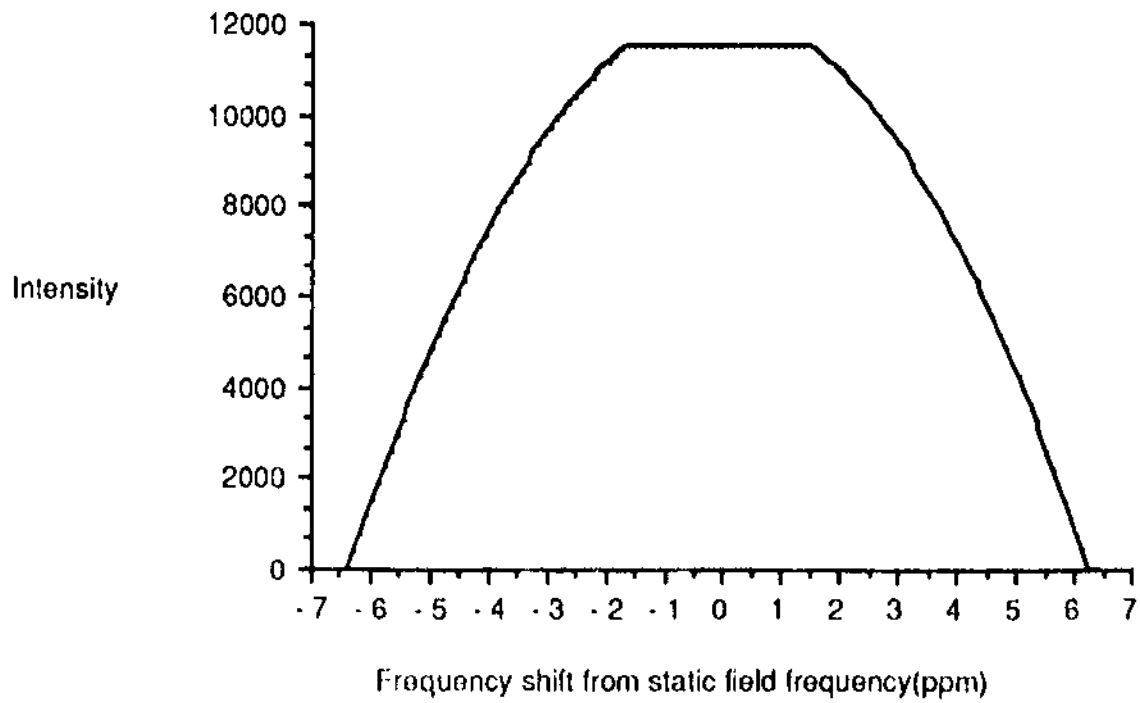Figure 5b: Relative dipole field value vs. distance along the x axis

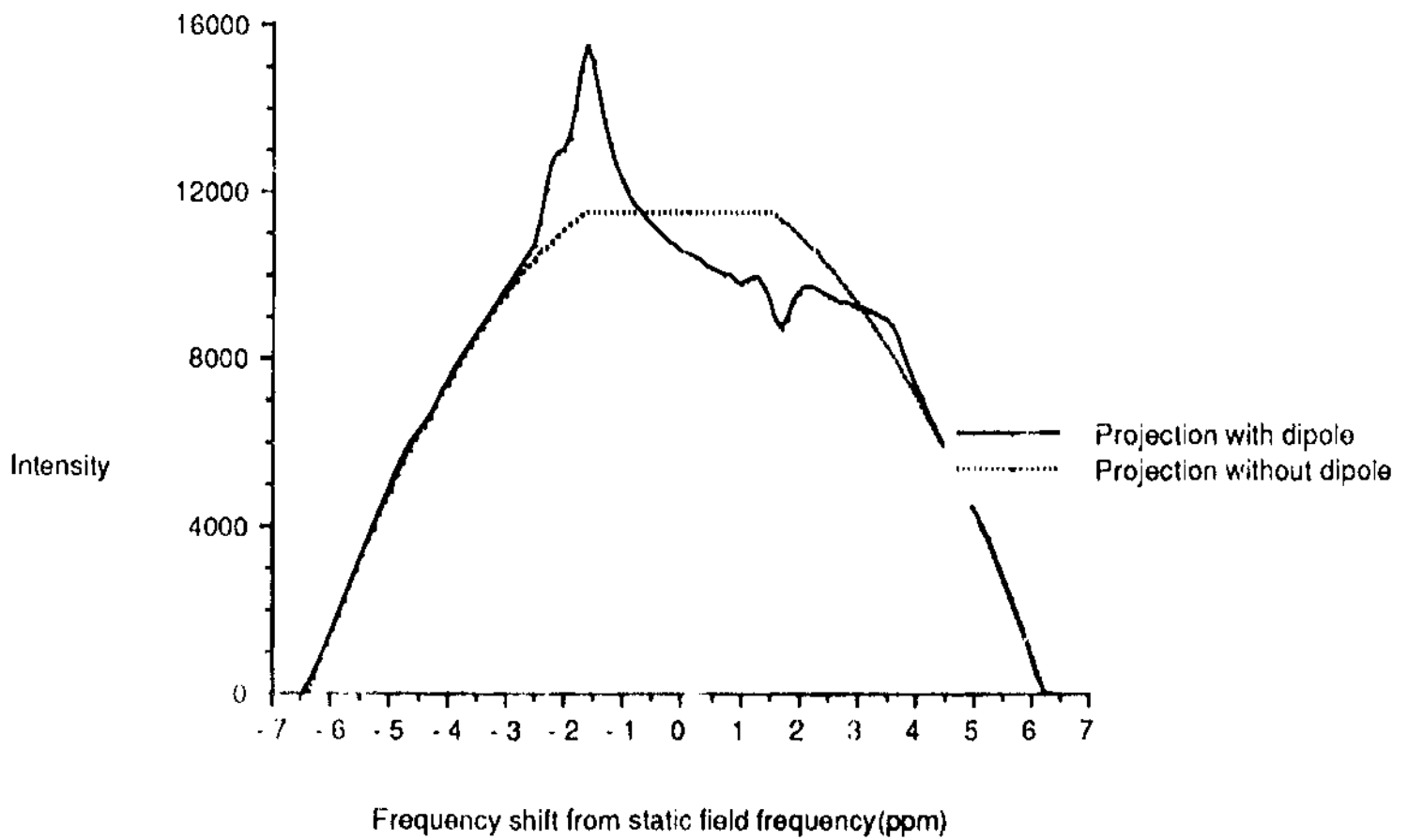Figure 6a: Calculated projection for hollow sphere

Figure 6b: Calculated projections along the z axis
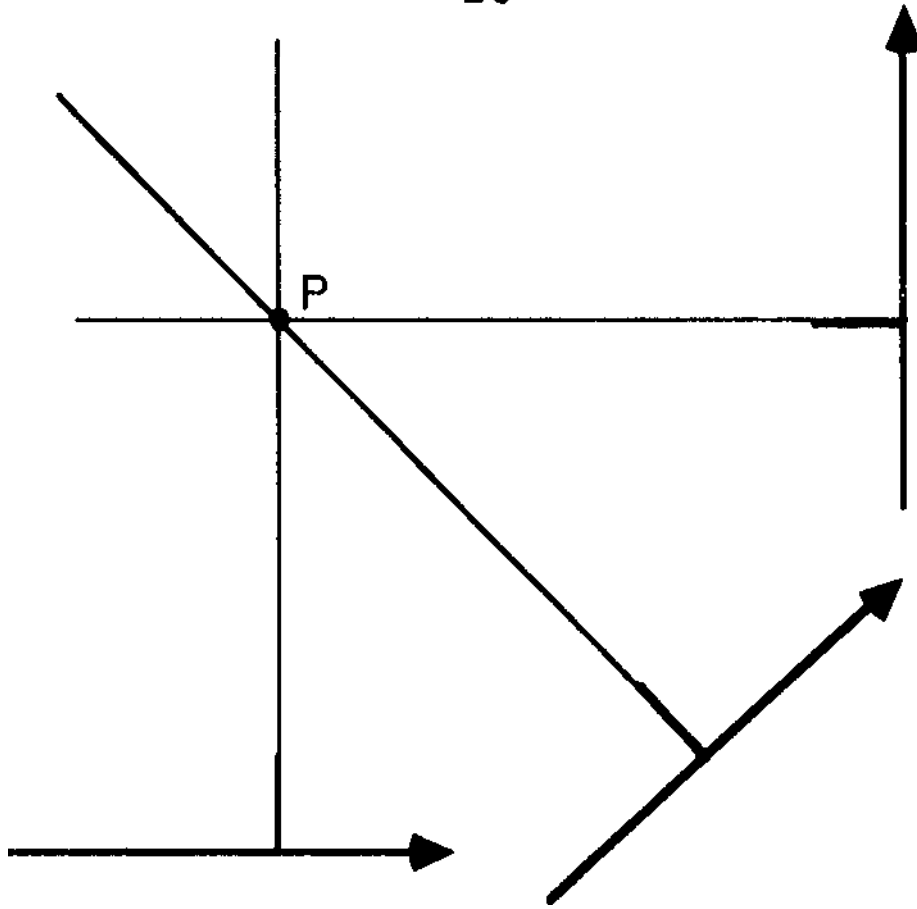with and without the dipole contribution

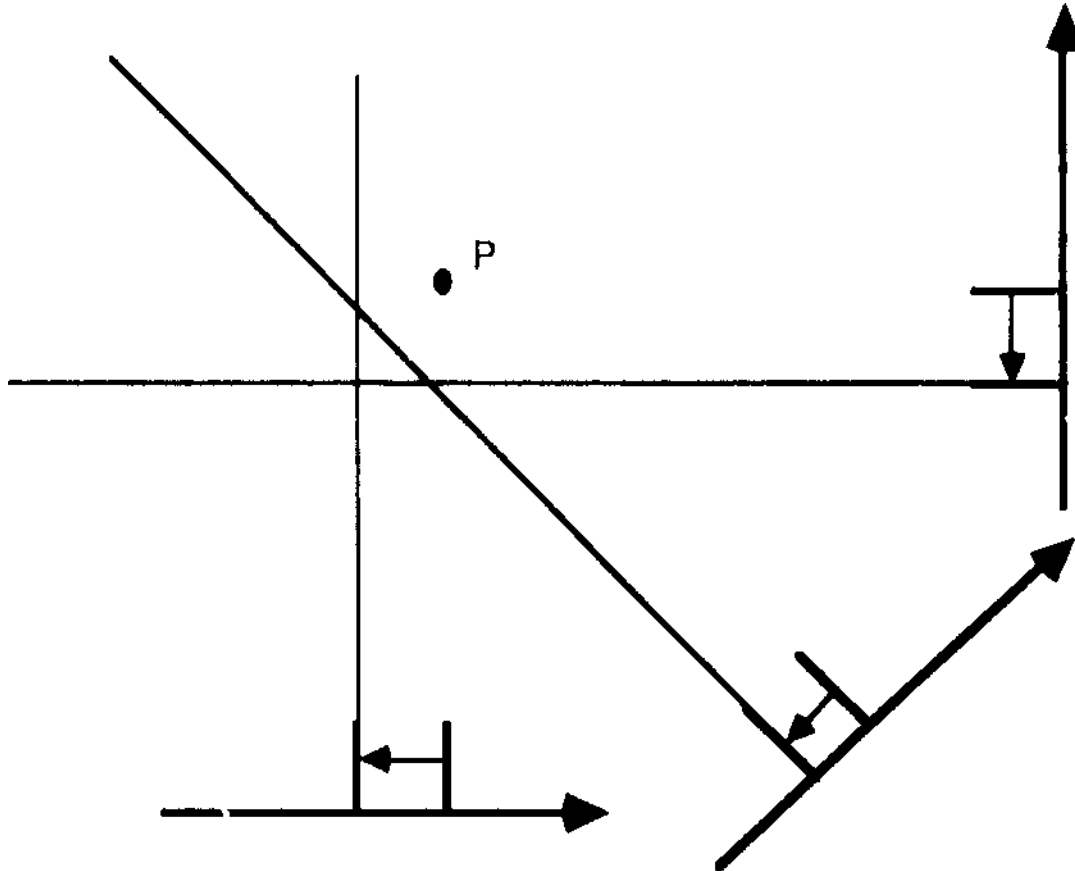Figure 7a: Intensity contributions converging in reconstruction space

Figure 7b: Shifted intensity contributions not converging in reconstruction space
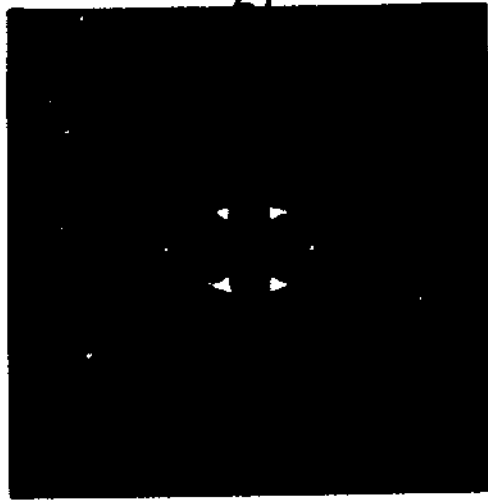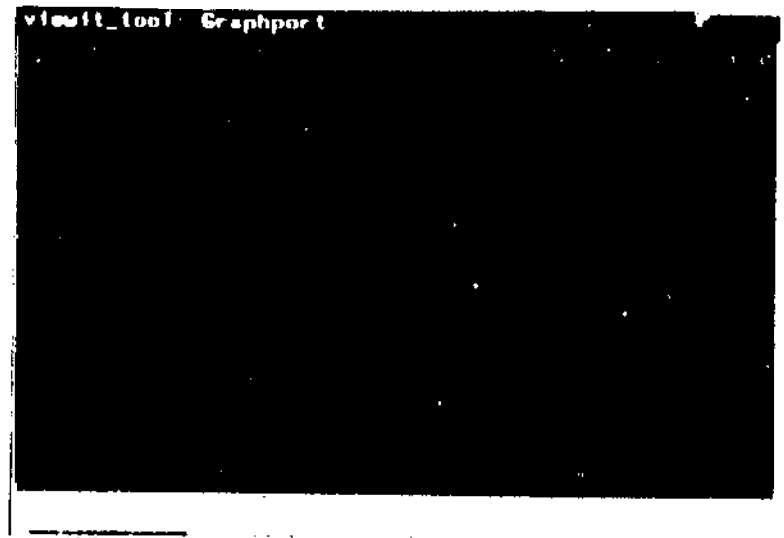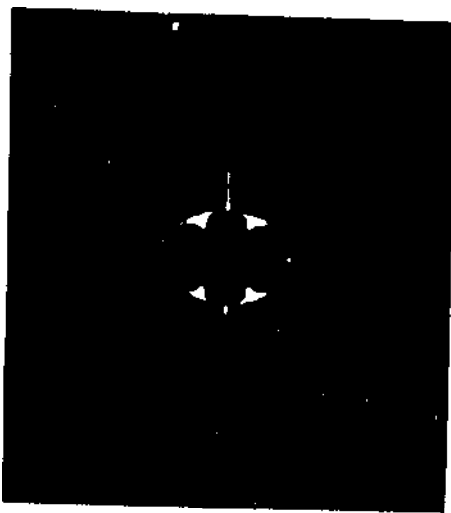
Figure 8: Simulated dipole artifact

Figure 9: Intensity profile at 90"

Figure10: Experimental dipole artifact

Appendix: Source Code for Simulation

```
/*****************************************/
This program computes frequency histograms equivalent to
projections for a sphere of permeability muin surrounded by a
spherical volume of permeability muex.  Constant values for static
field (bo in Gauss), gradient strength (G in Gauss/cm), gradient
reorientation step sizes for phi and theta (dphi and dtheta in
radians), relative volume permeabilities of internal and external
material (muin and muex in 1/cc), spatial increment (dr in cm),
radius of inner sphere (R in cm), and frequency  increment (dv in
ppm) must be in a file "pmtrs.h".
/*****************************************/


#include <stdio.h>
#include <math.h>
#include "pmtrs.h"

#define  thetadim  60
#define  rmax  4.0*R
#define  bdim    (int)  (rmax/dr)*2.0
#define  vdim    131
#define  pi 3.14159
#define  mu (muex - muin)/(2.0*muex + muin)
#define  Rcd pow(R,3.0)

float phig, sphig, cphig;
float thetag, sthetag, cthetag, x, y, r, z, f;
float c, b, vmin, vin, vv[vdim], v[vdim][thetadim+2], rg;
int a, m, n, o, p, q, g, d, e, h, i, j, l, aa, bb, cc, ee, dd, ff, locate(),;
FILE *out_file, *im_file, *fopen();

main()
{
/* open output files im_file contains histograms and out_file is
used as a test file to store intermediate values               */

    out_file=fopen("ffx","w");
    if(out_file==NULL)
      {fprintf(stdin,"ERROR- output file is not opened\n");
      exit(1);
    }                                28
```

```c
im_file= fopen("lh128","w");
if (im_file==NULL)
{
    fprintf(stdin,"ERROR-im_file not opened\n");
   exit(1);
}



/* input frequency values in array vv which defines frequency axis
value of vmin determines the lowest frequency value            */

for(o=0;o<vdim;o++)
{
   vin= (float) (o-64)*dv ;
  vv[o]=vin;
    fprintf(out_file,"%6f\n",vv[o]);
}



c= 0.0;

for(a=0;a<=thetadim/2 ;a++)         /*loops through theta 0-90deg */
{
for(p=0;p<vdim;p++)               /* initialize histogram values */
 v[p][a]=0.0;

x= -rmax;   z= -rmax; y= -rmax;   /* initialize spatial coordinates*/
r=hypot(hypot(x,y),z);


thetag= c*dtheta;      /* calculate theta value and its sin and cos */
 sthetag=sin(thetag);
 cthetag=cos(thetag);

phig= 0.0;
 sphig= sin(phig);
 cphig= cos(phig);

for(aa=0;aa<bdim;aa++)                  /*loops through z values*/
{
```

```
        z=-rmax+(float)aa*dr;
      for(bb=0;bb<bdim;bb++)                    /*loops through y values*/
    {

        y=-rmax+(float)bb*dr;
      for(cc=0;cc<bdim;cc++)                    /*loops through x values*/
      {

          x=-rmax+(float)cc*dr;

          if(r>=R && r<=rmax)        /* test if point is outside air bubble */
        {
          rg = x*sthetag*cphig + y*sthetag*sphig + z*cthetag;


          b= 0.0  ;/*-mu"Rcd*(2.0*pow(z,2.0)-pow(x,2.0)-
              pow(y,2.0))/pow(r,5.0);*/

        f = (b + G*rg/bo)*1.0e6;

        g=locate(vv,vdim,f,g);
        v[g][a]=v[g][a]+1.0;


        }
          r=hypot(hypot(x,y),z);
      }
          r=hypot(hypot(x,y),z);
    }
      r=hypot(hypot(x,y),z);
  }
    for(n=1;n<vdim-1;n++)
      fprintf(im_file,"%6f \n",v[n][a]);

    c=c+1.0;
    }

for(g=0;g<2;g++)                    /*three point linear averaging smoothing*/
{for(e=0;e<31;e++)
  {for(ee=1;ee<128;ee++)
    v[e][ee]=(v[e][ee-1]+v[e][ee]+v[e][ee+1])/3.0;
  }
}
```

```c
/*reproduce projections to get 3542 projections */

  for(ff=0;ff<31;ff++)
  {for(m=0;m<129;m++)
    fprintf(outfile,"%6f\n",v[ff][m]);
  }
  for(o=0;o<129;o++)
    fprintf(out_file,"%6f ",v[0][o]);
  fprintf(out_file,"\n");

  for(d=1;d<31;d++)
  {for(i=0;i<60;i++)
  {for(n=0;n<129;n++)
     fprintf(out_file,"%6f ",v[d][n]);

     fprintf(out_file,"\n");
  }
  }

  for(q=29;q>0;q--)
  {for(j=0;j<60;j++)
   {for(l=0;l<129;l++)
     fprintf(out_file,"%6f ",v[q][l]);

     fprintf(out_file,"\n");
  }
  }
  for(dd=0;dd<129;dd++)
    fprintf(out_file,"%6f ",v[0][dd]);

}


/*subroutine locate returns lower limit of intervalcontaining test
point or returns end values if the point is out of range*/

int  locate(xx,n,x,j)
float  xx[],x;
int  n,j;
{
  int  ascnd,ju,jm,jl;
```

```
 jl=0;
 ju=n;
 ascnd= xx[n-1] > xx[0];

 while (ju-jl > 1)
 {
   jm=(ju+jl) >> 1;
   if (x > xx[jm-1] == ascnd)
     jl=jm;
   else
     ju=jm;
 }
 j=jl;
 return(j);
}
```

```
/*  Input  file  "pmtrs.h"*/

#define  dphi  12.0*pi/180.0
#define  dtheta  3.0*pi/180.0
#define  dr  6.4e-4
#define  dv  0.100766
#define  bo  47000
#define  G  7.4
#define  muin  1.0
#define  muex  0.99999095
#define  R  0.01
```